THE JOURNAL OF PHYSICAL CHEMISTRY C

ARTICLE

pubs.acs.org/JPCC

# Mechanistic Analysis of Gas Enrichment in Gas−Water Mixtures near Extended Surfaces

Joonho Lee and N. R. Aluru*

Department of Mechanical Science and Engineering, Beckman Institute for Advanced Science and Technology, University of Illinois at Urbana−Champaign, Urbana, Illinois 61801, United States

**ABSTRACT:** We investigate gas enrichment near extended surfaces for gas−water mixtures using molecular dynamics simulations. We develop a detailed understanding of the various interactions that are responsible for gas enrichment by considering different gas−water mixtures and surfaces. We identify the significance of the solvent−induced potential on gas and show that both the solvent−induced potential and the gas−wall potential play an important role in gas enrichment. We perform a detailed thermodynamic analysis and discuss the significance of the entropic and enthalpic components of the solvent−induced potential for gas enrichment.

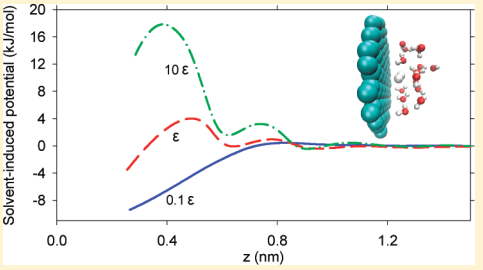


## I. INTRODUCTION

The interfacial structure of water near extended surfaces is an important problem as it can influence the physical and chemical phenomena in solutions. The presence of depletion layers and nanobubbles of water near extended hydrophobic surfaces has been studied for a long time.[1−4] Anomalous water structures near the surface can affect the hydrophobic interaction of apolar objects in solutions[5] and the slip behavior of water transport in hydrophobic channels.[6] Since solvation of gases in water at atmospheric pressure is a common phenomenon, it is important to consider the effects of the gases dissolved in water. For example, significant differences have been obtained between the presence and absence of dissolved gases in the strength and range of hydrophobic interaction.[7−10] Similarly, gas molecules forming droplets in (20,20) CNTs reduce the slip length of water transport.[11] On the other hand, in narrower tubes, such as in a (10,0) CNT, selectively adsorbed gas molecules from gas−water mixtures block water transport through the tube.[12,13] Even though gases dissolved in water can significantly influence the nanoscale behavior, gas distribution near an extended surface in the presence of gas−water mixtures has not been understood in great detail.

Gas enrichment (high gas concentration) has been observed in various simulations near the hydrophobic surface.[14−17] Dammer and Lohse[15] performed molecular dynamics simulations to understand gas concentration near the wall for gas−water mixtures. They used Lennard-Jones (L-J) particles to mimic water and gas molecules. The hydrophobicity of the surface was controlled by changing the L-J parameter, $\varepsilon$, between water and wall. They showed that the gas concentration near the wall depended on the hydrophobicity of the wall. Luzar and Bratko[17] reported that when they used the more accurate models for water and gas instead of L-J particles the dependency of the gas concentration on the hydrophobicity of the walls was not significant. Moreover, the physical origin and quantitative understanding of gas enrichment near a solid surface is not well−understood. To investigate these issues in great detail, we perform molecular dynamics simulations for different surfaces and develop a mechanistic understanding of gas enrichment by calculating the potential of mean force (PMF) and performing thermodynamic analysis.

The remainder of the paper is organized as follows. In section II, we introduce the methods used in the paper and calculate the excess free energy of the gases to estimate the solubility of each gas. These results are used for thermodynamic analysis of gases near surfaces. In section III, we calculate the free energy using the potential of mean force and develop a quantitative and physical understanding of gas enrichment. Finally, conclusions are presented in section IV.

## II. METHODS

We performed molecular dynamics simulations of gas−water mixtures near the surfaces with different interaction parameters to understand the enrichment of gas concentration near different surfaces. We consider different gas−water mixtures in order to understand the relative importance of various driving forces on gas enrichment. The simulations for $CO_2$−water and $H_2$−water mixtures are performed separately. The number ratio of water and gas molecules is 100:1 for all mixtures and surfaces considered. The number of the water molecules is $N_{wt}$ = 3000, and the number of the gas molecules is $N_{gas}$ = 30. We excluded the chemical reaction between $CO_2$ and water as a very small amount of the dissolved $CO_2$ reacts with water, and thus, this effect can be negligible.[16,18] For water, SPC/E water model is used.[19] The L-J parameters and electrostatic partial charges for the gas molecules ($CO_2$ and $H_2$) were taken from refs 17 and 20. We estimated the solubility of $CO_2$ and $H_2$ models[17,20−22] by the method discussed in ref 23, where a slab of liquid water (using SPC/E water

**Received:** June 4, 2011
**Revised:** August 2, 2011
**Published:** August 03, 2011

ACS Publications © 2011 American Chemical Society



dx.doi.org/10.1021/jp205260j | J. Phys. Chem. C 2011, 115, 17495–17502

model) is separated by vapor regions at 300 K. The solubility of $CO_2$ and $H_2$ in water using the models presented in this paper and their comparison to experimental data at 300 K is shown in Table 1. The graphene surface is positioned in the middle of the system, and the force-field parameters of the carbon atom are taken from ref 24. These parameters are listed in Table 2. Because the graphene structure is a smooth hexagonal plane without molecular level roughness, we can exclude the effects of wall properties caused by the configuration or roughness of the wall. A snapshot of the $CO_2$−water mixture near the graphene surface is shown in Figure 1. Two other surfaces are also considered for which the L-J parameter $\varepsilon$ is taken to be 0.1 and 10 times of the graphene $\varepsilon$ and the structure is the same as that of the graphene. The L-J parameters between different molecules were obtained by applying the Lorentz−Berthelot mixing rules, $\sigma_{ij} = (\sigma_{ii} + \sigma_{jj})/2$ and $\varepsilon_{ij} = (\varepsilon_{ii}\varepsilon_{jj})^{1/2}$. A cutoff distance of 1.2 nm is used for the L-J potential. Electrostatic interactions were computed by using the particle mesh Ewald method with a grid spacing of 0.15 nm. Periodic boundary conditions are applied in all three directions. Time integration was performed by using the leapfrog algorithm with a time step of 1.0 fs. The temperature of the system is controlled by Nosé-Hoover thermostat with the characteristic time of 0.1 ps.[25] The hydrostatic pressure of the system is maintained at 0.1 MPa for each case by using the Parrinello−Rahman scheme applied to the $z$ direction with a time constant of 0.1 ps and compressibility of $4.5 \times 10^{-5}$ bar$^{-1}$.[26] In order to obtain enough statistics, we performed simulation for about 50 ns in each case. The average volume of the system is slightly different for each gas−water mixture. Both $H_2$−water and $CO_2$−water systems are supersaturated with gas at 0.1 MPa pressure and 300 K. Since the supersaturated condition has considerable stability,[27] the system is maintained in a single phase. Simulations were performed using GROMACS 3.3.1.[28]

It is important to note that, among the many properties of the surfaces, hydrophobicity has been regarded as an important property for gas enrichment near the surface. However, controlling the hydrophobicity of surfaces is not trivial as it is usually a combined effect of the surface roughness, the charge distribution on the surface, etc. In this paper, we tried to exclude the diverse properties of the surface and focus on how the gas enrichment changes as the wall property changes. To consider realistic systems, we used the graphene surface and changed the property of the wall by varying the van der Waals parameters. Graphene is a monolayer of graphite, and we assumed that it is flat without corrugations.[29] Varying the van der Waals interaction parameters of the wall influences the gas−wall interaction and the water−wall interaction. By considering both effects, we analyze the effect of the change in the wall property on the gas concentration near the surface.

Before investigating the enrichment of gases near the surface via thermodynamic analysis, we need to evaluate the excess free energy of the gases, $CO_2$ and $H_2$, in bulk water at 300 K to check solvation free energy in bulk water. These bulk values will be used to compare the values near the surface. We performed simulations of 895 water molecules at 285, 300, and 315 K with pressure of 0.1 MPa and used each configuration to calculate the excess potential by the Widom insertion method.[30,31] In the Widom insertion method, after generating the random position of a virtual gas molecule in each configuration of water box, we compute $\exp(-\beta\Delta U)$, where $\Delta U$ is the potential energy difference between the systems before and after adding a virtual gas molecule, $\Delta U = U(N_{wt} + N_{gas}) - U(N_{wt})$, when $N_{gas} = 1$.

**Table 1. Solubility of Gas Models**

| | | molar ratio (gas/water) | |
|---|---|---|---|
| gas | vapor pressure (MPa) | simulation | experiment |
| $CO_2$ | 0.25 | $1.6 \times 10^{-3}$ | $1.5 \times 10^{-3}$ |
| $H_2$ | 0.58 | $10 \times 10^{-5}$ | $8 \times 10^{-5}$ |

**Table 2. Parameters for the LJ Potential and Charges**

| site | $\varepsilon$ (kJ/mol) | $\sigma$ (nm) | $q/e$ |
|---|---|---|---|
| C ($CO_2$) | 0.4058 | 0.3358 | 0.6172 |
| O ($CO_2$) | 0.7766 | 0.2836 | −0.3086 |
| H ($H_2$) | | | 0.4932 |
| center ($H_2$) | 0.2852 | 0.3038 | −0.9864 |
| C (graphene) | 0.2897 | 0.3390 | |
| O ($H_2O$) | 0.6302 | 0.3169 | −0.8476 |
| H ($H_2O$) | | | 0.4238 |

**Table 3. Excess Chemical Potentials of Gas Species at 300 K in Bulk Water**

| kJ/mol | $CO_2$ | $H_2$ |
|---|---|---|
| $\Delta\mu_{ex}$ | −0.50 | 8.82 |
| $\Delta\mu_{ex,entropy}$ | 20.97 | 8.24 |
| $\Delta\mu_{ex,enthalpy}$ | −21.47 | 0.58 |

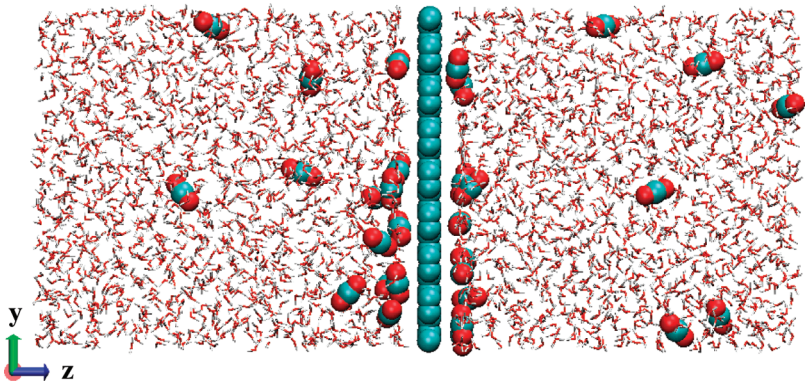


**Figure 1.** (a) Snapshot of the system (graphene and $CO_2$−water mixture).


dx.doi.org/10.1021/jp205260j |J. Phys. Chem. C 2011, 115, 17495–17502

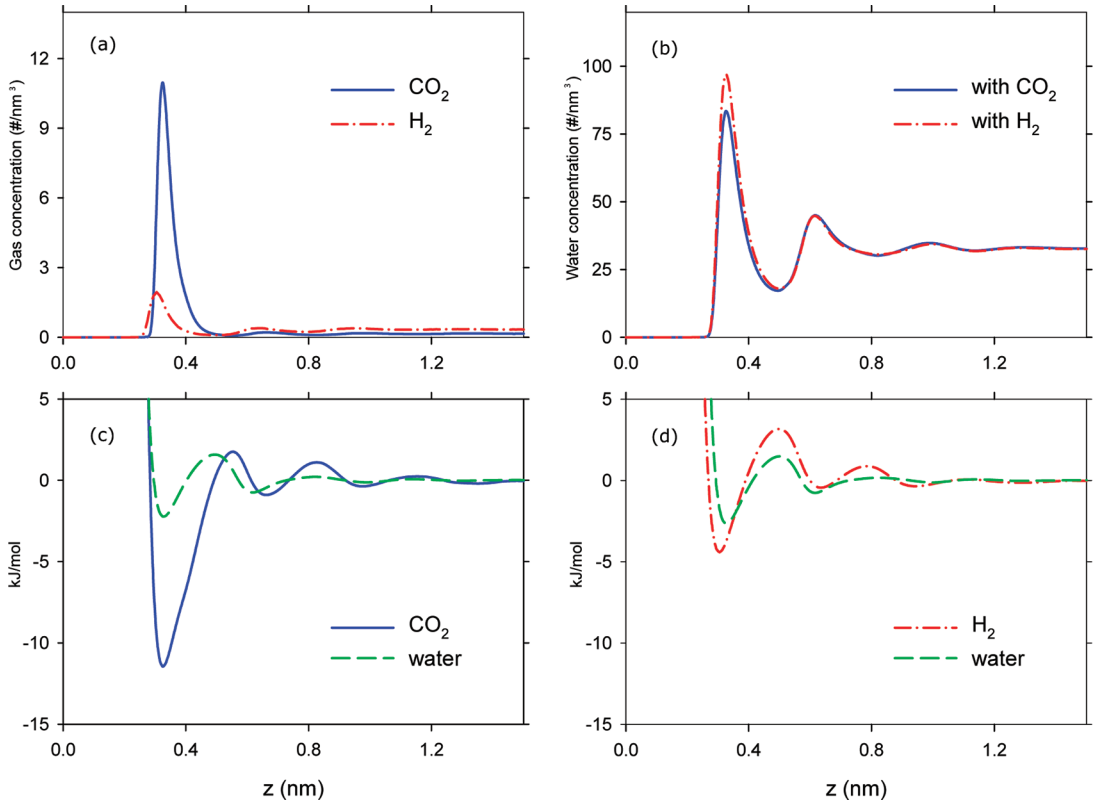


**Figure 2.** (a) Gas concentrations of $CO_2$−water and $H_2$−water mixtures near the graphene as a function of distance from the wall. (b) Water concentrations of $CO_2$−water and $H_2$−water mixtures near the graphene surface. (c) Total PMF of $CO_2$ and water of the $CO_2$−water mixture near the graphene as a function of distance from the wall. (d) Total PMF of $H_2$ and water of the $H_2$−water mixture near the graphene surface.

The excess chemical potential is an average over configurations defined as

$$\Delta\mu_{ex} = -kT \ln \frac{\langle V \int ds_{N+1} \exp(-\beta\Delta U)\rangle}{\langle V\rangle} \quad (1)$$

where $k$ is the Boltzmann constant, $T$ is the temperature of system, $\beta = 1/kT$, $V$ is the volume of the system, and the brackets $\langle ...\rangle$ indicate isothermal−isobaric averaging over the configurations. To thermodynamically quantify this potential energy, we evaluated the entropic, $-T\Delta s_{ex}$, and enthalpic, $\Delta h_{ex} = \Delta\mu_{ex} + T\Delta s_{ex}$, components by using the finite difference method

$$-\Delta s_{ex} \approx \frac{\Delta\mu_{ex}(T + \Delta T) - \Delta\mu_{ex}(T - \Delta T)}{2\Delta T} \quad (2)$$

based on the relationship $(\partial\mu/\partial T)_P = -\Delta s$ and the chemical potentials at 285, 300, and 315 K. Table 3 shows that the excess free energy of $CO_2$ is negative and the excess free energy of $H_2$ is positive ($CO_2$ is more soluble than $H_2$). These values are reasonable when compared to the data in refs 23 and 32. The calculation reveals that the entropic component of the excess potential is unfavorable to gas solvation in water.[32] The positive entropic component represents the reduction of entropy of water at 300 K because an inserted gas molecule occupies a certain volume in water.[5] The enthalpic component of the excess chemical potential of $CO_2$ is negative. The negative enthalpic component of the free energy can be regarded as the attraction between a gas molecule and water molecules, which acts as the favorable factor for gas solvation. On the other hand, the enthalpic component of $H_2$ is positive but, it is small enough to be not too unfavorable. Based on these characteristics, we analyze the difference of thermodynamic components near the surface.

## III. RESULTS AND DISCUSSION

The gas and water concentrations as a function of distance from the graphene surface for $CO_2$−water and $H_2$−water mixtures are shown in Figure 2, panels a and b. In both cases, gas enrichment near the graphene surface is observed. The peak $CO_2$ concentration near the graphene is much bigger than that of $H_2$ concentration (see Figure 2a) and the position of the peak of $H_2$ concentration ($z = 0.31$ nm) is slightly closer to the wall than that of the $CO_2$ concentration ($z = 0.33$ nm). The magnitude of the first peak of water concentration in the $CO_2$−water mixture case is slightly smaller than that in the $H_2$−water mixture case (see Figure 2b). This reduction of the first peak of the water concentration in $CO_2$−water case is caused by the high concentration of $CO_2$ near the graphene surface. Since the number of gas molecules is 1/100 of the number of water molecules, the overall distribution of water is not significantly altered by the distribution of the gas.

Both water and gas have a high concentration peak near the graphene surface. However, the magnitude of the gas concentration near the graphene surface normalized by its bulk concentration is higher than that of water in both $CO_2$−water and $H_2$−water mixtures. This can be estimated by the free energy difference of the gas and water as a function of the distance from


dx.doi.org/10.1021/jp205260j |J. Phys. Chem. C 2011, 115, 17495–17502

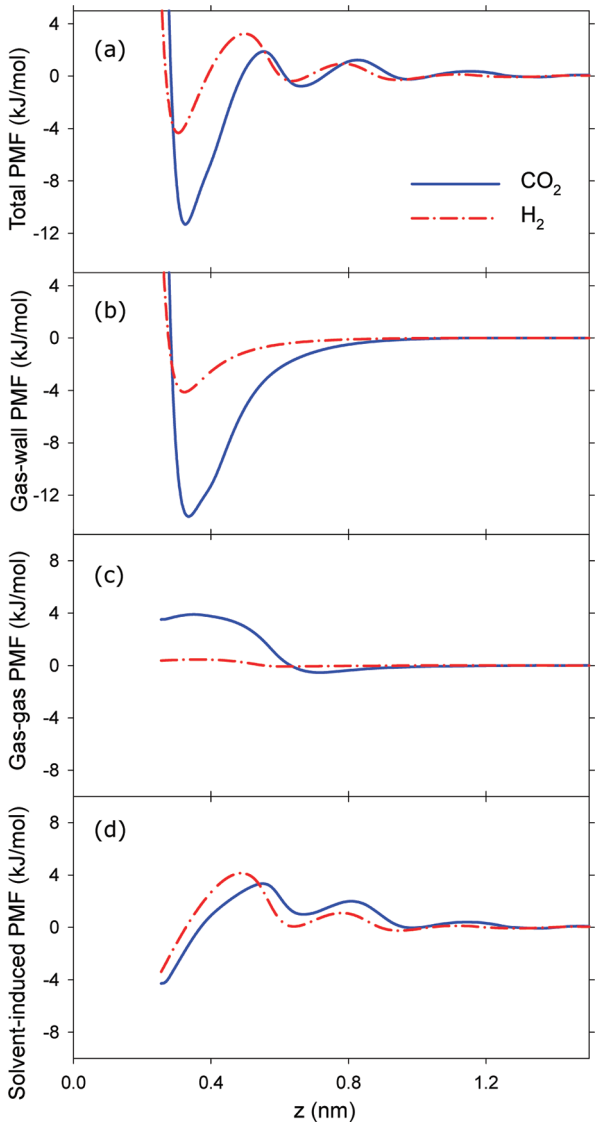


**Figure 3.** (a) Total PMF of gases for $CO_2$−water and $H_2$−water mixtures near the graphene as a function of distance from the wall. (b) Gas−wall potentials for $CO_2$−water and $H_2$−water mixtures near the graphene. (c) Gas−gas interactions for $CO_2$−water and $H_2$−water mixtures near the graphene. (d) Solvent-induced potentials on gases for $CO_2$−water and $H_2$−water mixtures near the graphene.

**Table 4. Free Energies of Gas Species at the Minima of the Total PMF**

| | graphene | | wall with $0.1\varepsilon_{grap}$ | |
|---|---|---|---|---|
| kJ/mol | $CO_2$ | $H_2$ | $CO_2$ | $H_2$ |
| $\Delta PMF_{total}$ | −11.3 | −4.4 | −8.5 | −9.0 |
| $\Delta PMF_{gas-wall}$ | −13.4 | −3.8 | −3.9 | −1.0 |
| $\Delta PMF_{gas-gas}$ | 3.9 | 0.4 | 1.0 | 1.1 |
| $\Delta w$ | −1.8 | −1.0 | −5.6 | −9.1 |
| $\Delta w_{entropy}$ | −9.9 | −13.0 | −10.7 | −8.7 |
| $\Delta w_{enthalpy}$ | 8.1 | 12.0 | 5.1 | −0.4 |

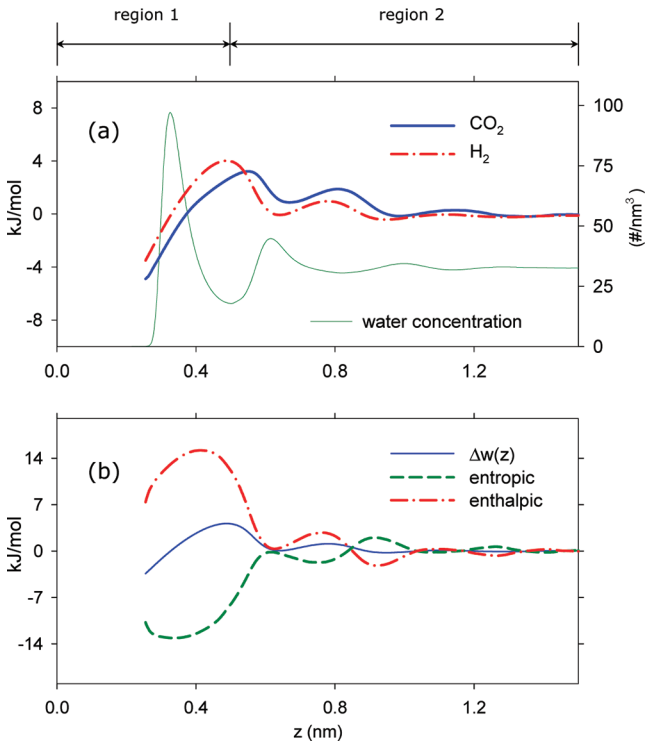


**Figure 4.** (a) Solvent-induced potentials on the gas for $CO_2$−water and $H_2$−water mixtures and water concentration as a function of distance from the surface. (b) Solvent-induced potential, its entropic component and enthalpic component as a function of distance from the surface for $H_2$−water mixture at 300 K.

the graphene surface. Potential of mean force $\Delta PMF_{total}(z)$ is calculated by integrating the mean force profiles along the $z$ axis and the ends of both sides of the system are set as the reference position where the $\Delta PMF_{total}(z)$ is zero (see Figure 2, panels c and d). The force profile is obtained by averaging the force on the molecules at various z positions along the direction orthogonal to the wall.[33] Corresponding to the density distributions of water and gases, $\Delta PMF_{total}(z)$ shows the lower free energy of $CO_2$ over water near the graphene surface. In the case of $H_2$−water, $\Delta PMF_{total}(z)$ of $H_2$ is slightly lower than that of water at their minimum positions, even though $\Delta PMF_{total}(z)$ of $H_2$ is higher than that of water in the region from $z$ = 0.4 nm to 0.8 nm as shown in Figure 2d. Considering the competition between water and gas near the surface, the free energy of gases at the first peak near the surface is lower than the free energy of water.

The contribution of water to the free energy change of gases, which we denote as the solvent-induced potential $\Delta w(z)$,[34−36] is obtained by subtracting the gas−gas PMF and the gas−wall PMF from the total PMF of gas as $\Delta w(z) = \Delta PMF_{total}(z) - \Delta PMF_{gas-wall}(z) - \Delta PMF_{gas-gas}(z)$ (see Figure 3, panels a−d). The various components at the minimum positions of the total PMF profile (the most stable position of the gas from the surface, $z$ = 0.33 nm for $CO_2$ and $z$ = 0.31 nm for $H_2$) are shown in Table 4. The gas−wall interaction energy of $CO_2$ is about four times stronger than that of $H_2$. Compared to the difference between the gas−wall potentials for $CO_2$ and $H_2$, the difference in the solvent-induced potentials on gas for $CO_2$ and $H_2$ cases is small. In the case of $CO_2$, the strong gas−wall interaction contributed primarily to the stabilization of the contact configuration compared to the solvent-induced


dx.doi.org/10.1021/jp205260j |J. Phys. Chem. C 2011, 115, 17495–17502

component. In the case of $H_2$, the gas−wall interaction of $H_2$ is smaller compared to that of $CO_2$. Therefore, the solvent-induced potential becomes comparable to the gas−wall interaction and makes the total PMF of $H_2$ lower than the total PMF of water near the graphene.

To understand the $\Delta w(z)$ profiles further, we analyzed $\Delta w(z)$, as shown in Figure 4a, by dividing the region near the surface into regions 1 and 2. Region 1 is within the water monolayer distance from the graphene surface, and the rest of the region is identified as region 2. The solvent-induced potential decreases rapidly as the gas molecule approaches the wall in region 1 and the unfavorable barriers to gas enrichment are found in region 2. We decomposed the solvent-induced potential at 300 K to entropic $-T\Delta S(z)$ and enthalpic $\Delta H(z)$ components and estimated them in both regions. The entropic and enthalpic components are computed, analogous to the excess chemical potential, by using the finite difference method and $\Delta w(z)$ profiles at 285, 300, and 315 K. Figure 4b shows the entropic and enthalpic components of the solvent-induced potential on $H_2$ for the $H_2$−water mixture. Since the solvent-induced potential $\Delta w(z)$ follows the change of the enthalpic component of $\Delta w(z)$ in region 2, the enthalpic component is dominant over the entropic component in this region. The enthalpic component of the solvent-induced potential is primarily due to the direct interaction with water.[5] The strong layering of water near the graphene surface causes the enthalpic component to increase, and this forms the unfavorable potential barrier for gas enrichment near the surface. As the gas approaches closer to the graphene surface and is within region 1, the entropic component becomes dominant and this makes $\Delta w(z)$ negative. The enthalpic and entropic contribution of $\Delta w(z)$ at the minima of the total PMF indicates that the entropic component of $\Delta w(z)$ contributes to high concentration of gas near the wall in region 1 (see Table 4). This explanation for enrichment of $H_2$ near the graphene surface is also applicable to the enrichment of $CO_2$ in the $CO_2$−water case.

Since the dissolved gas and its enrichment near the surface can affect the water structure near the surface (e.g., formation of depletion layer, bubbles, etc.[4,9]), we also investigated the effect of

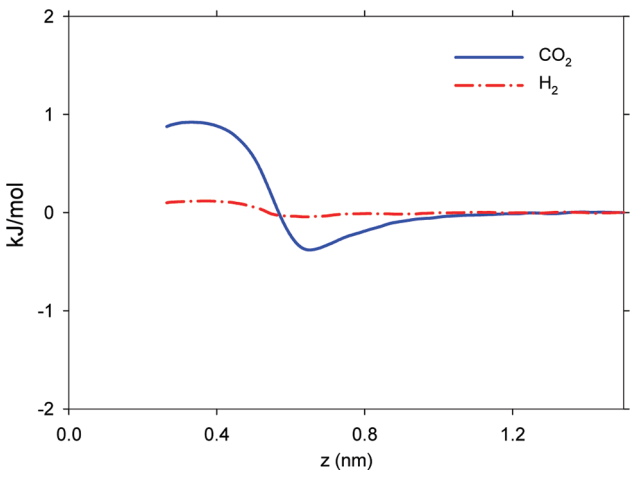


**Figure 5.** Gas contribution to water PMF for $CO_2$−water and $H_2$−water mixtures as a function of distance from the graphene surface.

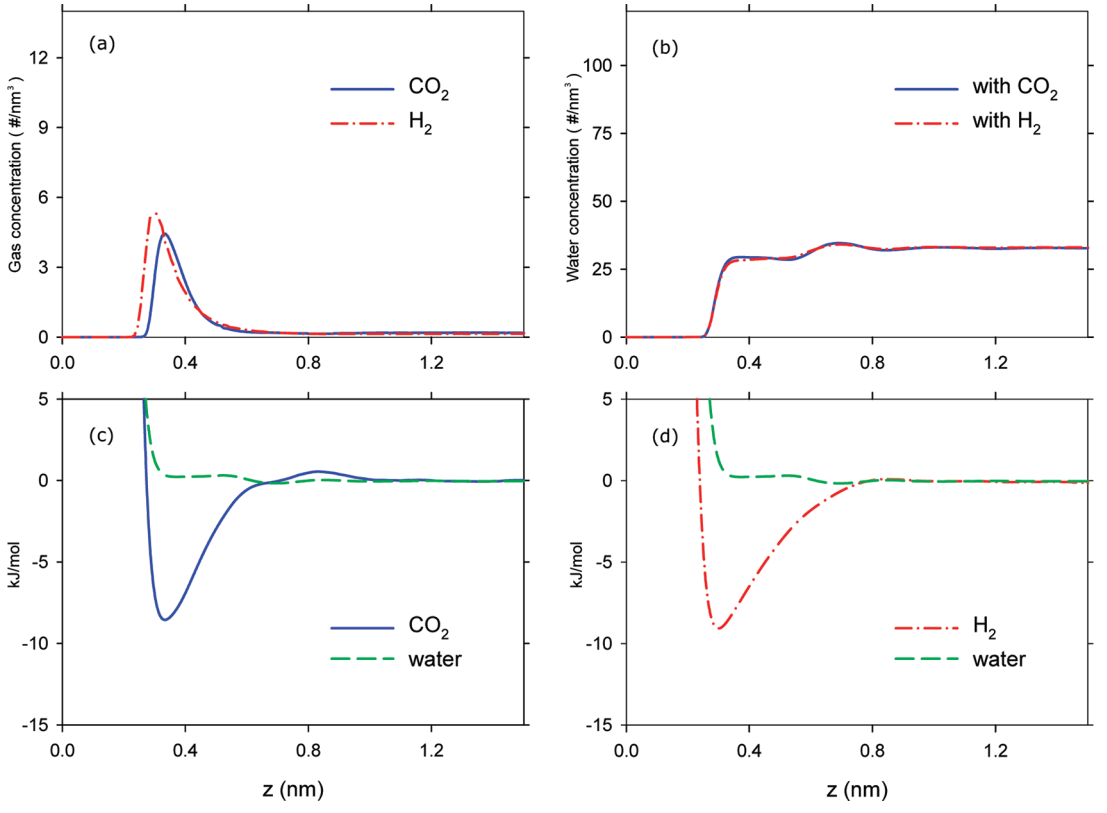


**Figure 6.** (a) Gas concentration of $CO_2$−water and $H_2$−water mixtures near the fictitious wall as a function of distance from the wall. (b) Water concentration of $CO_2$−water and $H_2$−water mixtures near the fictitious wall. (c) Total PMF of $CO_2$ and water for $CO_2$−water mixture near the fictitious wall as a function of distance from the wall. (d) Total PMF of $H_2$ and water for $H_2$−water mixture near the fictitious wall.


dx.doi.org/10.1021/jp205260j |J. Phys. Chem. C 2011, 115, 17495–17502

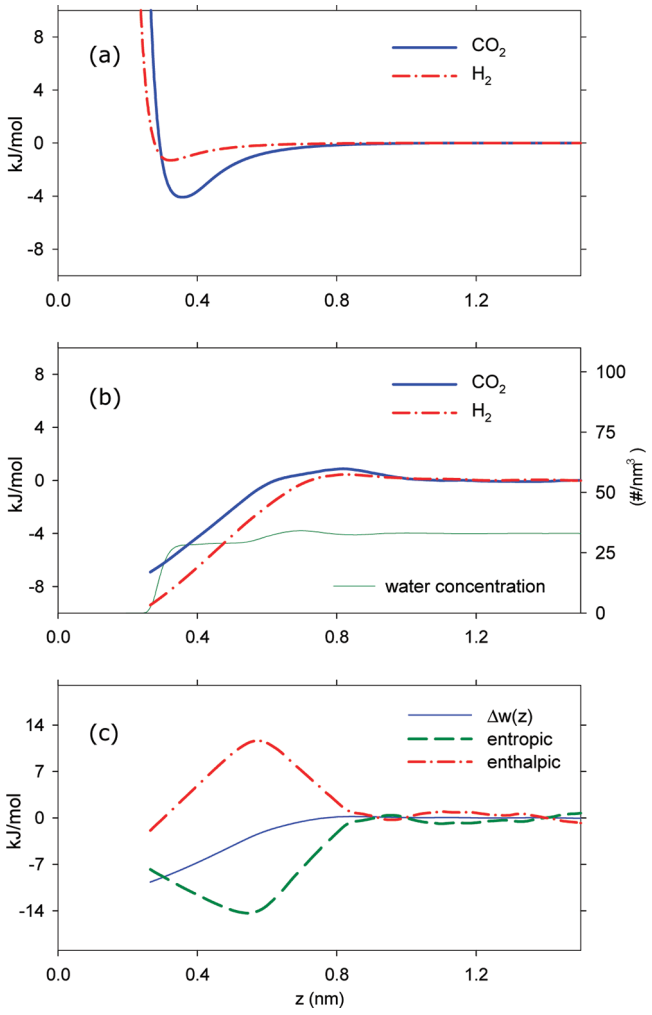


**Figure 7.** (a) Gas−wall potentials for $CO_2$−water and $H_2$−water mixtures near the fictitious wall. (b) Solvent-induced potential on the gas for $CO_2$−water and $H_2$−water mixtures and water concentration for $H_2$−water mixture near the fictitious wall. (c) Solvent-induced potential, its entropic component and enthalpic component for $H_2$−water mixture near the fictitious wall at 300 K.

gas on the water distribution near the surface. To investigate the free energy change of water by gas enrichment near the graphene surface, we calculate the contribution of gas to the PMF of water as shown in Figure 5. Since the number of gas molecules is small (1/100 of that of water molecules), the effect of gas on the PMF of water is small compared to the total PMF of water. The PMF calculation shows that the free energy change of water is affected (even though it is small) by gas concentration near the graphene surface. The contribution of gas to water PMF increases with the concentration of gas near the surface.

To understand how the gas enrichment changes with the property of the surface, we next considered a fictitious wall with the L-J parameter, $\varepsilon_{fict}$, to be 0.1 times of that of graphene, $\varepsilon_{grap}$ ($\varepsilon_{fict} = 0.1\varepsilon_{grap}$) and the structure is the same as that of the graphene. Since the L-J interactions between different molecules are based on the Lorentz−Berthelot mixing rules in this paper, decreasing the value of $\varepsilon$ of the wall parameter makes the water−wall and the gas−wall interactions weaker at the same time. The simulations were performed using these modified parameters, and all other simulation details are identical as described above for the graphene case. Gas enrichment is observed near the fictitious wall as shown in Figure 6a. Although the concentration of $CO_2$ near the graphene is higher than that of $H_2$ near the graphene, the concentration of $H_2$ is higher than that of $CO_2$ near the fictitious wall with concentration peaks located at $z$ = 0.34 nm for $CO_2$ and $z$ = 0.30 nm for $H_2$ (compare Figures 2a and 6a). The difference between $CO_2$ and $H_2$ concentration near the fictitious wall is much smaller than that of the graphene case. Consistent with the gas concentrations, the PMF profiles of gases (Figure 6, panels c and d) are similar and the difference in the minimum values of the PMF (at the minima) is 0.5 kJ/mol. This difference is much smaller than that of the graphene case (−6.9 kJ/mol). In addition, the fluctuation in the total PMF of gas near the fictitious wall is not significant compared to the graphene case. For water concentration, the strong water layering near the graphene surface disappears near the fictitious wall because of the decreasing interaction between water and wall (see Figure 6b). The concentration of the first layer of water is reduced and almost equal to the bulk concentration.

We decomposed the $\Delta PMF_{total}(z)$ of the gas in the fictitious wall case, using the same approach as described for the graphene case, and the results are shown in Figure 7 and Table 4. Compared to the graphene case, the gas−wall interactions of both gas species are less negative (smaller in magnitude) at the minima of total PMF and their solvent-induced potential are more negative (larger in magnitude) as shown in Figure 7, panels a and b. So, the solvent-induced potential becomes the dominant component for gas enrichment near the fictitious wall. Furthermore, in terms of the entropic and enthalpic components of $\Delta w(z)$ at the minima of the total PMF, the entropic components of $\Delta w(z)$ are changed by −0.8 kJ/mol for $CO_2$ and 4.3 kJ/mol for $H_2$ from the values of the graphene case (see Table 4). The enthalpic components decreased by 3.0 kJ/mol for $CO_2$ and 12.4 kJ/mol for $H_2$ from the values of the graphene case. The reduction of the unfavorable enthalpic component makes the solvent-induced potential, $\Delta w(z)$, more favorable for gas enrichment and this reduction is attributed to the suppression of water layers near the surface.

Finally, we also investigate gas enrichment in the case where the $\varepsilon$ of the wall is increased to 10 times that of graphene, $10\varepsilon_{grap}$. Increasing $\varepsilon$ of the wall strengthens the gas−wall and the water−wall interactions. In this case, we observed that the concentration of $CO_2$ near the wall has increased while that of the $H_2$ has decreased compared to the graphene wall case. In the case of the graphene wall and the fictitious wall with $0.1\varepsilon_{grap}$, the solvent-induced potential helps gas enrichment near the wall. However, as the interaction between water and the wall becomes much stronger, more stable layering of water is established and the solvent-induced potential prevents gas enrichment near the wall. Since $CO_2$ has stronger interaction with the wall compared to water, te $CO_2$−wall interaction is able to overcome the unfavorable solvent-induced potential and causes higher concentration of $CO_2$ near the wall than the graphene case. On the contrary, the $H_2$−wall interaction is weaker compared to the water−wall interaction, hence, the unfavorable solvent-induced potential is dominant near the wall and the $H_2$ concentration near the wall is reduced compared to the graphene case. This relation between gas concentration and $\varepsilon$ of the wall is consistent with the previous cases as shown in Figure 8.


dx.doi.org/10.1021/jp205260j |J. Phys. Chem. C 2011, 115, 17495–17502

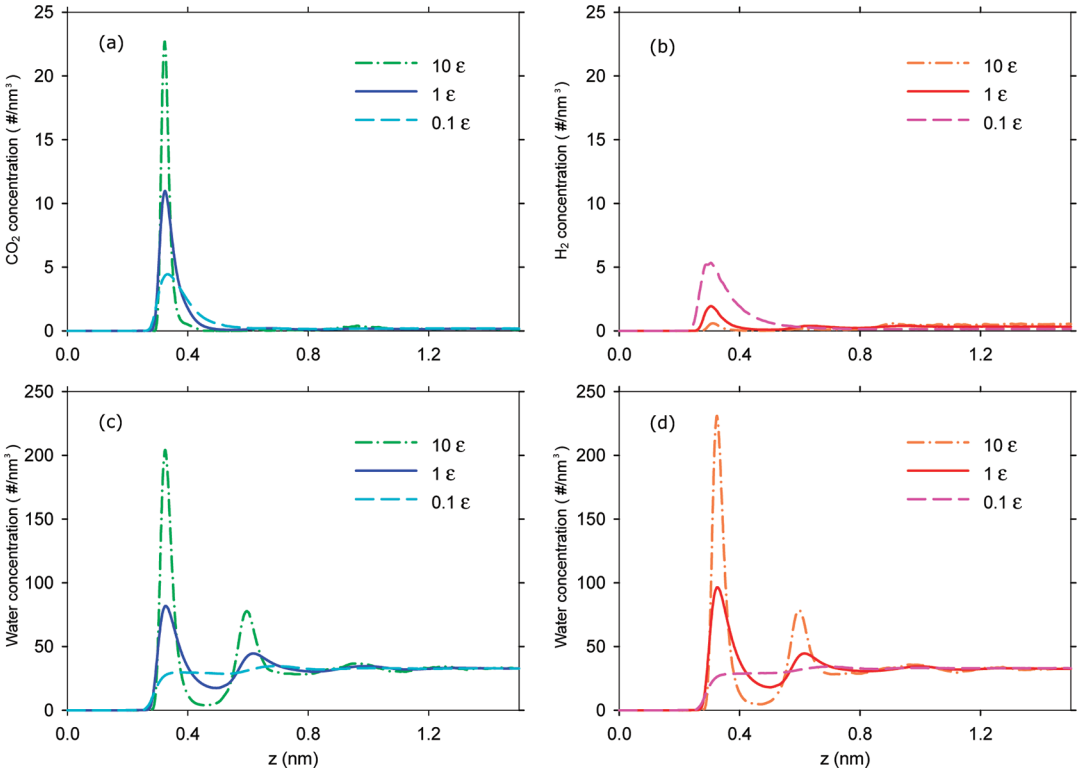


**Figure 8.** (a) $CO_2$ concentration of $CO_2$−water mixture near the walls with different $\varepsilon$. (b) $H_2$ concentration of $H_2$−water mixture near the walls with different $\varepsilon$. (c) Water concentration of $CO_2$−water mixture near the walls with different $\varepsilon$ (d) Water concentration of $H_2$−water mixture near the walls with different $\varepsilon$.

## IV. CONCLUSIONS

Gas enrichment of gas−water mixtures near extended surfaces depends on the type of the gas species and the nature of the wall (hydrophobic, hydrophilic, etc.). Although the gas−wall interaction is considered to be an important force giving rise to gas enrichment near surfaces, we show that the force exerted by water on the gas molecules, referred to as the solvent-induced potential, can be quite significant in some cases giving rise to gas enrichment. The decomposition of the solvent-induced potential into its entropic and enthalpic components reveals that the entropic component near the surface favors gas enrichment, whereas the enthalpic component is unfavorable. The significance of the solvent-induced potential on gas enrichment can depend on the type of the gas−water mixture and the extended surface.

## AUTHOR INFORMATION

### Corresponding Author

*E-mail: aluru@illinois.edu.

## ACKNOWLEDGMENT

This research was supported by NSF under Grant Nos. 0120978, 0328162, 0810294, 0852657, and 0915718.

## REFERENCES

(1) Ishida, N.; Inoue, T.; Miyahara, M.; Higashitani, K. *Langmuir* **2000**, *16*, 6377–6380.
(2) Tyrrell, J. W. G.; Attard, P. *Phys. Rev. Lett.* **2001**, *87*, 176104.
(3) Steitz, R.; Gutberlet, T.; Hauss, T.; Klösgen, B.; Krastev, R.; Schemmel, S.; Simonsen, A. C.; Findenegg, G. H. *Langmuir* **2003**, *19*, 2409–2418.
(4) Doshi, D. A.; Watkins, E. B.; Israelachvili, J. N.; Majewski, J. *Proc. Natl. Acad. Sci.* **2005**, *102*, 9458–9462.
(5) Chandler, D. *Nature* **2005**, *437*, 640–647.
(6) Granick, S.; Zhu, Y.; Lee, H. *Nat. Mater.* **2003**, *2*, 221–227.
(7) Cristenson, H. K.; Claesson, P. M. *Science* **1988**, *239*, 390–392.
(8) Craig, V. S. J.; Ninham, B. W.; Pashley, R. M. *Langmuir* **1999**, *15*, 1562–1569.
(9) Wennerstrm, H. *J. Phys. Chem. B* **2003**, *107*, 13772–13773.
(10) Meyer, E. E.; Lin, Q.; Israelachvili, J. N. *Langmuir* **2005**, *21*, 256–259.
(11) Kotsalis, E. M.; Walther, J.; Koumoutsakos, P. *Int. J. Multiphase Flow* **2004**, *30*, 995–1010.
(12) Kalra, A.; Hummer, G.; Garde, S. *J. Phys. Chem. B* **2004**, *108*, 544–549.
(13) Lee, J.; Aluru, N. R. *Appl. Phys. Lett.* **2010**, *96*, 133108.
(14) Wallqvist, A.; Berne, B. J. *Chem. Phys. Lett.* **1988**, *145*, 26–32.
(15) Dammer, S. M.; Lohse, D. *Phys. Rev. Lett.* **2006**, *96*, 206101.
(16) Luzar, A.; Bratko, D. *J. Phys. Chem. B* **2005**, *109*, 22545–22552.
(17) Bratko, D.; Luzar, A. *Langmuir* **2008**, *24*, 1247–1253.
(18) Somasundaram, T.; in het Panhuis, M.; Lynden-Bell, R. M.; Patterson, C. H. *J. Chem. Phys.* **1999**, *111*, 2190–2199.
(19) Berendsen, H. J. C.; Grigera, J. R.; Straatsma, T. P. *J. Phys. Chem.* **1987**, *91*, 6269–6271.
(20) Alavi, S.; Ripmeester, J. A.; Klug, D. D. *J. Chem. Phys.* **2005**, *123*, 024507.
(21) Murthy, C. S.; Singer, K.; McDonald, I. R. *Mol. Phys.* **1981**, *44*, 135–143.
(22) Harris, J. G.; Yung, K. H. *J. Phys. Chem.* **1995**, *99*, 12021–12024.
(23) Somasundaram, T.; Lynden-Bell, R. M.; Patterson, C. H. *Phys. Chem. Chem. Phys.* **1999**, *1*, 143–148.

(24) Chen, G.; Guo, Y.; Karasawa, N.; Goddard, W. A., III *Phys. Rev. B* **1993**, *48*, 13959–13970.
(25) Nosé, S. *Mol. Phys.* **1984**, *52*, 255–268.
(26) Parrinello, M.; Rahman, A. *J. Appl. Phys.* **1981**, *52*, 7182–7190.
(27) Hemmingsen, E. A. *Science* **1970**, *167*, 1493–1494.
(28) Lindahl, E.; Hess, B.; van der Spoel, D. *J. Mol. Model.* **2001**, *7*, 306–317.
(29) Geim, A. K. *Science* **2009**, *324*, 1530–1534.
(30) Widom, B. *J. Chem. Phys.* **1963**, *39*, 2808–2812.
(31) Frenkel, D.; Smit, B. *Understanding Molecular Simulation-From Algrithms to Applications*, 2nd ed.; Academic Press: San Diego, CA, 2001.
(32) Paschek, D. *J. Chem. Phys.* **2004**, *120*, 6674–6690.
(33) Kjellander, R.; Greberg, H. *J. Electroanal. Chem.* **1998**, *450*, 233–251.
(34) Bulone, D.; Martorana, V.; San Biagio, P. L.; Palma-Vittorelli, M. B. *Phys. Rev. E* **1997**, *56*, 4939–4942.
(35) Ghosh, T.; Garcia, A. E.; Garde, S. *J. Chem. Phys.* **2002**, *116*, 2480–2486.
(36) Sobolewski, E.; Makowski, M.; Czaplewski, C.; Liwo, A.; Oldziej, S.; Scheraga, H. A. *J. Phys. Chem. B* **2007**, *111*, 10765–10774.